

Semiclassical theory of a quantum pump

Saar Rahav and Piet W. Brouwer

Laboratory of Atomic and Solid State Physics, Cornell University, Ithaca 14853, USA.

(Dated: September 7, 2017)

In a quantum charge pump, the periodic variation of two parameters that affect the phase of the electronic wavefunction causes the flow of a direct current. The operating mechanism of a quantum pump is based on quantum interference, the phases of interfering amplitudes being modulated by the external parameters. In a ballistic quantum dot, there is a minimum time before which quantum interference can not occur: the Ehrenfest time τ_E . Here we calculate the current pumped through a ballistic quantum dot if τ_E is comparable to the mean dwell time τ_D . Remarkably, we find that the pumped current has a component that is not suppressed if $\tau_E \gg \tau_D$.

PACS numbers: 73.23.-b, 05.45.Mt, 73.50.Pz

I. INTRODUCTION

A suitably chosen periodic perturbation of an electronic device may result in a direct current, even when the system is not biased. In the adiabatic limit, when the applied perturbation is slow in comparison to the escape rate to external contacts, the electronic state is the same after each period while a finite charge is transferred through the device during each cycle. Such devices are called charge pumps. Charge pumps have been proposed as current sources and minimal-noise current standards,^{1,2,3} as well as diagnostic tools to monitor how mesoscopic devices respond to changing external parameters.^{4,5,6,7,8,9,10}

In this article, we consider a so-called ‘quantum charge pump’. In a quantum pump, the external perturbation affects the phases of the electron wavefunctions only, not the classical dynamics of the electrons.^{4,5,6,9,11,12,13} Such a scenario can be realized in a ballistic quantum dot, where small variations of shape-defining gate voltages or of an applied magnetic field are known to significantly affect the electronic phase while leaving classical trajectories unaffected. Such a device, with two shape-distorting gate voltages to drive the current, was built by Switkes *et al.*⁴ Although the pumped current in the original experiment of Ref. 4 was obscured by rectification effects,¹⁴ ‘quantum pumping’ was demonstrated in a later experiment, be it not in the adiabatic regime.¹⁵

Microscopically, the current in a quantum pump is the result of quantum interference: two classical trajectories initially a microscopic distance apart (a Fermi wavelength) split and rejoin, with a phase difference that depends on the applied perturbation. Indeed, if the mean dwell time τ_D in the device exceeds the dephasing time τ_ϕ , the pumped current is suppressed.^{16,17} Aleiner and Larkin have pointed out that, in a ballistic quantum dot (as in any quantum system with a well-defined classical counterpart for which the dynamics is chaotic), there is another time that governs quantum interference:^{18,19} the Ehrenfest time τ_E . The Ehrenfest time is the time during which two classical trajectories initially a Fermi wavelength apart are separated to a macroscopic distance (the width of the contacts or the size of the quantum dot) by

the chaotic classical dynamics.^{20,21} The Ehrenfest time is given by

$$\tau_E = \frac{1}{\lambda} \ln N + \text{const}, \quad (1)$$

where λ is the Lyapunov exponent of the classical dynamics in the quantum dot and N denotes the total number of channels in the contacts. The constant in Eq. (1) is independent of N . While the dephasing time governs the suppression of interference for long dwell times, the Ehrenfest time is the minimum time needed for the appearance of interference effects.

Being an interference effect, the current pumped through a ballistic chaotic quantum dot is a random function of any parameter that affects quantum phases, such as the shape of the dot or the applied magnetic field (taken at a reference point during the cycle). Therefore, one typically considers averages and fluctuations of the current, taken with respect to an ensemble of dots with slightly varying shape or with respect to a range of magnetic field strengths. Since the ensemble-averaged current $\langle I \rangle = 0$, the magnitude of the pumped current is measured through the second moment $\langle I^2 \rangle$. With a few exceptions,^{13,22} random matrix theory has been the preferred framework for a statistical theory of quantum-dot based charge pumps.^{11,23,24,25,26,27} Random matrix theory describes the regime $\tau_E \ll \tau_D$, in which quantum effects occur on a time scale much shorter than the mean dwell time τ_D in the quantum dot. In this article, we are interested in a quantum pump in the regime in which τ_E and τ_D are comparable. Since, typically, $\tau_D \lambda \gg 1$, this requires that we consider the classical limit $N \gg 1$.

A remarkably wide range of τ_E -dependences has been reported in the literature for various quantum interference effects in ballistic quantum dots. Weak localization, the quantum interference correction to the ensemble-averaged conductance in the presence of time-reversal symmetry, is suppressed $\propto \exp(-\tau_E/\tau_D)$ if τ_E is large.^{18,28,29,30} On the other hand, conductance fluctuations have no τ_E dependence,^{31,32,33} whereas the quantum correction to the spectral form factor of a closed quantum dot with broken time-reversal symmetry exists for finite τ_E only,^{34,35} being absent in the random matrix

limit $\tau_E \rightarrow 0$.³⁶ The main result of the present article is that current pumped in a quantum pump has yet another τ_E -dependence,

$$\langle I^2 \rangle = \frac{1}{2}(1 + e^{-2\tau_E/\tau_D})\langle I^2 \rangle_{\text{RMT}}, \quad (2)$$

where $\langle I^2 \rangle_{\text{RMT}}$ is the prediction of random matrix theory.

We calculate the Ehrenfest-time dependence of the pumped current using a semiclassical theory in which the pumped current is expressed as a sum over classical trajectories in the quantum dot. Our theory goes beyond a previous semiclassical theory of quantum pumps by Martinez-Mares *et al.*,²² who did not consider the role of the Ehrenfest time. Whereas Ref. 22 calculated the pumped current in the ‘diagonal approximation’, in which only pairs of identical classical trajectories are considered, we also include the leading off-diagonal terms in the sum over classical trajectories. In this respect, our theory builds on previous work by Richter and Sieber³⁷ and Heusler *et al.*,³⁸ who developed a systematic way to include off-diagonal terms in trajectory sums of the weak localization correction to the dot’s conductance and other quantum interference corrections to transport. Unlike the diagonal approximation, which is known to violate current conservation, the present version of the semiclassical theory is fully current conserving.

In Sec. II we express the pumped current in terms of a sum over classical trajectories. This section closely follows Ref. 22. The sum over classical trajectories, which gives the final result (2), is then performed in Sec. III. We compare the theoretical predictions to numerical simulations in Sec. IV and conclude in Sec. V.

II. SEMICLASSICAL THEORY OF A QUANTUM PUMP

The geometry under consideration is shown in Fig. 1. For definiteness, we consider a ballistic chaotic quantum dot coupled to two electron reservoirs via ballistic point contacts. The quantum dot has two holes. Slow periodic variations of the magnetic flux through each of the holes change the phases of wavefunctions, not the classical trajectories. Both holes are ‘macroscopic’: their size is large in comparison to the Fermi wavelength λ_F and their boundary is smooth.

We assume that the variation of the fluxes is adiabatic, with period $2\pi/\omega$ much larger than either the dwell time or the Ehrenfest time. In the adiabatic regime, the time-averaged current I_L through the left contact can be expressed in terms of the $N \times N$ scattering matrix S of the quantum dot,¹¹

$$I_L = \frac{e\omega}{2\pi} \int_{\mathcal{A}} d\phi_1 d\phi_2 \Pi^L(\phi_1, \phi_2),$$

$$\Pi^L(\phi_1, \phi_2) = \frac{1}{\pi} \text{Im} \sum_{\nu=1}^N \sum_{\mu=1}^{N_1} \frac{\partial S_{\mu\nu}^*}{\partial \phi_1} \frac{\partial S_{\mu\nu}}{\partial \phi_2}. \quad (3)$$

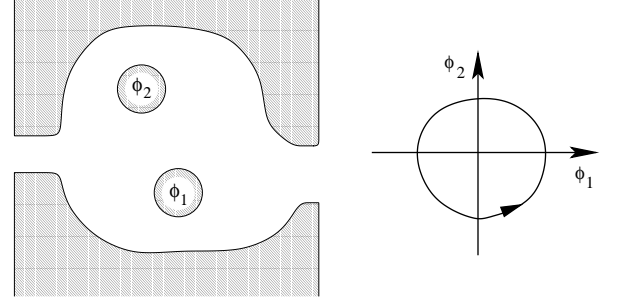


FIG. 1: Left: Schematic drawing of the quantum pump under consideration. The quantum pump consists of a ballistic quantum dot with two holes, through which a time-dependent magnetic flux ϕ is applied. The classical dynamics in the dot is assumed to be chaotic. Right: pumping cycle in flux-space.

Here ϕ_j is the flux through hole j , $j = 1, 2$, measured in units of the flux quantum hc/e , and the integral in Eq. (3) is taken over the area enclosed in (ϕ_1, ϕ_2) -space in one pumping cycle, see Fig. 1. The number of channels in the left and right contacts are N_1 and N_2 , respectively, and $N = N_1 + N_2$. In Eq. (3) we assumed zero temperature. The current through the right-contact reads

$$I_R = \frac{e\omega}{2\pi} \int_{\mathcal{A}} d\phi_1 d\phi_2 \Pi^R(\phi_1, \phi_2),$$

$$\Pi^R(\phi_1, \phi_2) = \frac{1}{\pi} \text{Im} \sum_{\nu=1}^N \sum_{\mu=N_1+1}^N \frac{\partial S_{\mu\nu}^*}{\partial \phi_1} \frac{\partial S_{\mu\nu}}{\partial \phi_2}. \quad (4)$$

Current conservation implies

$$I = I_L = -I_R, \quad (5)$$

so that

$$\Pi^L = -\Pi^R. \quad (6)$$

The key point of the semiclassical approach is to express the scattering matrix S as a sum over classical trajectories γ ,^{39,40,41}

$$S_{\mu\nu} = \frac{1}{\sqrt{N\tau_D}} \sum_{\gamma} A_{\gamma} e^{i\frac{\mathcal{S}_{\gamma}}{\hbar}}, \quad (7)$$

where γ starts at a contact with transverse momentum compatible with lead mode ν and ends with transverse momentum compatible with mode μ . (The modes $\mu = 1, \dots, N_1$ are in the left lead and the modes $\mu = N_1 + 1, \dots, N$ are in the right lead.) Further \mathcal{S}_{γ} is the classical action (which includes Maslov phases) and A_{γ} is the stability amplitude. The classical action is modified by the presence of the fluxes ϕ_1 and ϕ_2 as

$$\mathcal{S}(\gamma) = \mathcal{S}_0(\gamma) + \hbar[\phi_1 W_1(\gamma) + \phi_2 W_2(\gamma)], \quad (8)$$

where $W_j(\gamma)$ is the winding number of the trajectory γ around the hole j , $j = 1, 2$. We'll be interested in the

regime $\phi_j \ll 1$, and $W_j \gg 1$, for which the discreteness of the winding numbers does not play a role. Substituting Eqs. (7) and (8) into Eqs. (3) and (4), we arrive at²²

$$\begin{aligned}\Pi^L &= \frac{4\pi}{N\tau_D} \sum_{\nu=1}^N \sum_{\mu=1}^{N_1} \sum_{\gamma_1, \gamma_2} A_{\gamma_1} A_{\gamma_2} W_1(\gamma_1) W_2(\gamma_2) \\ &\quad \times \sin[(\mathcal{S}_{\gamma_2} - \mathcal{S}_{\gamma_1})/\hbar], \\ \Pi^R &= \frac{4\pi}{N\tau_D} \sum_{\nu=1}^N \sum_{\mu=N_1+1}^N \sum_{\gamma_1, \gamma_2} A_{\gamma_1} A_{\gamma_2} W_1(\gamma_1) W_2(\gamma_2) \\ &\quad \times \sin[(\mathcal{S}_{\gamma_2} - \mathcal{S}_{\gamma_1})/\hbar],\end{aligned}\quad (9)$$

where both γ_1 and γ_2 are compatible with modes ν and μ upon entrance and exit, respectively.

In the remainder of this article we limit ourselves to bilinear response, $I \propto \mathcal{A}$. For bilinear response, the fluctuations of the kernels Π^L and Π^R can be neglected when performing the integral over the enclosed area \mathcal{A} in (ϕ_1, ϕ_2) -space, so that it is sufficient to calculate the average and variance of the kernels Π^L and Π^R in order to find the average and variance of the pumped current I ,

$$\langle I \rangle = \frac{e\omega\mathcal{A}}{2\pi} \langle \Pi^L \rangle = -\frac{e\omega\mathcal{A}}{2\pi} \langle \Pi^R \rangle \quad (10)$$

$$\langle I^2 \rangle = \frac{e^2\omega^2\mathcal{A}^2}{4\pi^2} \langle (\Pi^L)^2 \rangle = -\frac{e^2\omega^2\mathcal{A}^2}{4\pi^2} \langle \Pi^L \Pi^R \rangle. \quad (11)$$

In the semiclassical framework, this means that we can neglect the dependence of the classical actions \mathcal{S}_{γ_j} on the variations of the parameters ϕ_1 and ϕ_2 in the sines in Eq. (9).

Before we can perform the summation over classical trajectories necessary to calculate $\langle I^2 \rangle$ we must specify the statistics of the winding numbers W_1 and W_2 . For a quantum dot with chaotic classical dynamics, one may assume that the two winding numbers $W_1(\gamma)$ and $W_2(\gamma)$ are statistically uncorrelated, and that the average winding number is zero,

$$\langle W_j(\gamma) \rangle = 0, \quad j = 1, 2. \quad (12)$$

For the variance of the winding number we take⁴²

$$\langle W_j(\gamma)^2 \rangle = C_j t, \quad j = 1, 2, \quad (13)$$

where the coefficients C_j depend on the size and shape of the quantum dot and on the location of the hole j , $j = 1, 2$, but not on the Ehrenfest time and t is the duration of the trajectory γ . For a chaotic quantum dot, one may also assume that the winding numbers $W_j(\gamma_1)$ and $W_j(\gamma_2)$ of different trajectories γ_1 and γ_2 are uncorrelated, $j = 1, 2$, except if there exist strong classical correlations between the two trajectories. Strong classical correlations exist if the two trajectories are within a phase space distance c , where c is a cut-off below which the chaotic classical dynamics in the quantum dot can be linearized. If two trajectories are correlated for only a

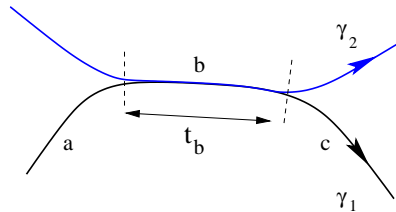


FIG. 2: (Color online) Schematic drawing of two partially correlated trajectories. The true trajectories are piecewise straight with specular reflection off the dot's boundaries.

part of their duration, as shown schematically in Fig. 2, only the duration t_b of the correlated segment contributes to the average of the product of the winding numbers,

$$\langle W_j(\gamma_1) W_j(\gamma_2) \rangle = C_j t_b, \quad j = 1, 2. \quad (14)$$

Although our theory is formulated for a quantum pump where the current is driven by time-dependent magnetic fluxes, the mathematical framework to describe other geometries, *e.g.* a pump in which current is driven by shape changes, is identical.²² For generic perturbations of a chaotic quantum dot the parameters still enter the classical action as a Gaussian random process, and the actions of different trajectories will have statistically uncorrelated dependences on the parameters. In that sense, our theory applies to arbitrary perturbations, not only time-dependent magnetic fluxes. (The only exception is a pump in which a gate voltage is changed uniformly in the quantum dot. A similar separation between ‘generic’ perturbations and a uniform gate voltage shift exists in the random matrix description of quantum pumps.^{11,24,26})

III. SUMMATION OVER CLASSICAL TRAJECTORIES

The semiclassical framework and the statistics of the winding numbers outlined in the previous section is the same as that used in a previous semiclassical theory of quantum pumps by Martinez-Mares, Lewenkopf, and Mucciolo.²² In Ref. 22, the fourfold sum over classical trajectories required to calculate the current variance is evaluated in the ‘diagonal approximation’, in which the four trajectories contributing $\langle I^2 \rangle$ are taken pairwise equal. Although Ref. 22 reports agreement between semiclassics and random matrix theory, the use of the diagonal approximation to calculate the current variance $\langle I^2 \rangle$ is problematic because it violates the unitarity relation (6): In the diagonal approximation, one has $\langle \Pi^L \Pi^R \rangle = 0$, while $\langle (\Pi^L)^2 \rangle \neq 0$. The diagonal approximation also fails to account for the fact that the variance of the pumped current does not depend on the presence or absence of time-reversal symmetry.^{11,23}

Problems with the diagonal approximation are not limited to the semiclassical theory of a quantum pump. In

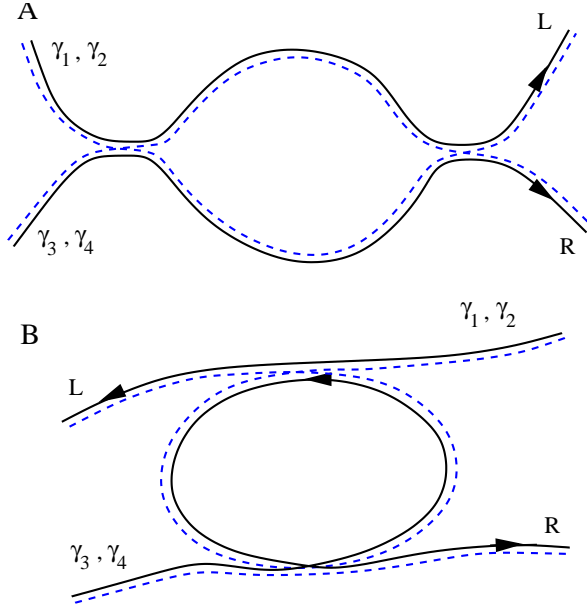


FIG. 3: (Color online) Schematic drawing of trajectory configurations of types A (top) and B (bottom) that generate the pumped current. Type A consists of all quadruples of classical trajectories with two separated small-angle encounters. Type B consists of all quadruples of classical trajectories for which two (or more) of the trajectories revolve around a periodic orbit. If the Ehrenfest time is much smaller than the mean dwell time, the pumped current is carried by trajectories of type A. If $\tau_E \gg \tau_D$, the current is carried by trajectories of type B.

fact, the diagonal approximation is well known to fail at providing a current-conserving description of other quantum interference effects, such as the weak localization correction to the conductance and universal conductance fluctuations.⁴³ For weak localization, this problem was solved by Richter and Sieber, who were able to include the relevant off-diagonal configurations of classical trajectories into the trajectory sum.³⁷ Below, we use a generalization of Richter and Sieber's technical innovation^{33,38,44,45} to perform the trajectory sums required for a current-conserving semiclassical theory of a quantum pump.

Since the two winding numbers W_1 and W_2 are statistically uncorrelated and have zero average, the trajectory sum in Eq. (9) immediately gives $\langle \Pi^L \rangle = \langle \Pi^R \rangle = 0$, and hence

$$\langle I \rangle = 0. \quad (15)$$

In order to calculate the average of the squared current, it is technically most convenient to use the second equality in Eq. (11). Using the semiclassical expression (9), one

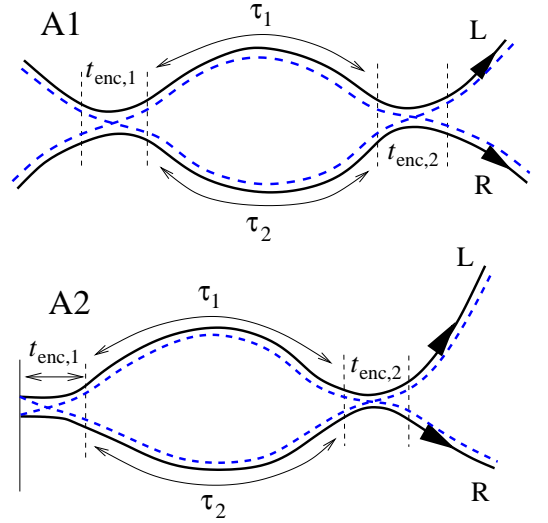


FIG. 4: (Color online) Trajectories of type A without and with correlated entry into the quantum dot (top and bottom, respectively).

has

$$\begin{aligned} \langle \Pi^L \Pi^R \rangle &= \frac{16\pi^2}{N^2 \tau_D^2} \sum_{\mu, \rho=1}^N \sum_{\nu=1}^{N_1} \sum_{\sigma=N_1+1}^N \sum_{\gamma_1, \gamma_2, \gamma_3, \gamma_4} \\ &\times \langle A_{\gamma_1} A_{\gamma_2} A_{\gamma_3} A_{\gamma_4} \\ &\times W_1(\gamma_1) W_2(\gamma_2) \sin[(\mathcal{S}_{\gamma_2} - \mathcal{S}_{\gamma_1})/\hbar] \\ &\times W_1(\gamma_3) W_2(\gamma_4) \sin[(\mathcal{S}_{\gamma_4} - \mathcal{S}_{\gamma_3})/\hbar] \rangle. \end{aligned} \quad (16)$$

The non-vanishing contributions to the current variance are from quadruples of trajectories for which the two action differences in the sine functions are almost identical, resulting in a non-oscillatory contribution to the trajectory sum. However, this alone does not ensure a finite contribution to $\langle I^2 \rangle$: In addition, the ensemble averages of the winding numbers should not vanish. This means that the trajectory pairs γ_1 and γ_3 , and γ_2 and γ_4 should be correlated for (at least) part of their duration. However, since these trajectories exit the dot in different contacts, they can not be identical.

The configurations of classical trajectories that meet these requirements are the same as the trajectories that contribute to conductance fluctuations.³³ They are shown in Fig. 3. The first type (labeled “A”) consists of two pairs of trajectories that undergo two separate small-angle encounters. Between the encounters and the contacts γ_1 and γ_2 , and γ_3 and γ_4 are pairwise equal (up to quantum uncertainties). Between the two encounters, γ_1 is paired with γ_3 or γ_4 , while γ_2 is paired with the remaining trajectory, γ_4 or γ_3 . The second type of trajectories (labeled “B”) contains a closed loop, which is traversed one (extra) time by two of the four trajectories. Below we discuss both contributions separately. Since the calculations closely follow the calculations of the conductance fluctuations, we refer to Ref. 33 for details of the formalism, and here restrict ourselves to those

parts of the calculation where we differ from Ref. 33.

A. contributions of type A

Within the configurations of type A, one distinguishes trajectories for which the first small-angle encounter fully resides inside the quantum dot, such that the entrance of the pairs trajectories γ_1 and γ_2 , and γ_3 and γ_4 is uncorrelated, and a configuration of trajectories in which the first small-angle encounter touches the entrance contact, so that all four trajectories enter the dot together. The

two situations are shown in Fig. 4. Since γ_1 and γ_2 exit through the left contact, whereas γ_3 and γ_4 exit through the right contact, the second encounter must fully reside inside the quantum dot in all cases. We refer to the two cases shown in Fig. 4 as “A1” and “A2”.

The durations of the encounters, defined as the time during which the phase space distance between the trajectories is less than a classical cut-off scale c , are denoted $t_{\text{enc},1}$ and $t_{\text{enc},2}$, as depicted in Fig. 4. The durations of the uncorrelated stretches between the encounters are denoted by τ_1 and τ_2 . We then expand

$$4 \sin[(\mathcal{S}_{\gamma_2} - \mathcal{S}_{\gamma_1})/\hbar] \sin[(\mathcal{S}_{\gamma_4} - \mathcal{S}_{\gamma_3})/\hbar] = e^{i(\mathcal{S}_{\gamma_2} - \mathcal{S}_{\gamma_1} + \mathcal{S}_{\gamma_3} - \mathcal{S}_{\gamma_4})/\hbar} - e^{i(\mathcal{S}_{\gamma_2} - \mathcal{S}_{\gamma_1} + \mathcal{S}_{\gamma_4} - \mathcal{S}_{\gamma_3})/\hbar} + \text{c.c.} \quad (17)$$

and find quadruples of trajectories γ_1 , γ_2 , γ_3 , and γ_4 for which the exponents in Eq. (17) are small. Between the encounter regions and the contacts, γ_1 and γ_2 , and γ_3 and γ_4 are paired, resulting in only a small contribution to the action differences in Eq. (17). In order to ensure that the contribution from the stretch between the encounters is small as well, one pairs γ_1 with γ_3 and γ_2 with γ_4 between the encounters for the first term in Eq. (17), and γ_1 with γ_4 and γ_2 with γ_3 for the second term. In the former case $\langle W_1(\gamma_1)W_1(\gamma_3) \rangle = C_1(t_{\text{enc},1} + t_{\text{enc},2} + \tau_1)$ and $\langle W_2(\gamma_2)W_2(\gamma_4) \rangle = C_2(t_{\text{enc},1} + t_{\text{enc},2} + \tau_2)$. In the latter case, one has $\langle W_1(\gamma_1)W_1(\gamma_3) \rangle = C_1(t_{\text{enc},1} + t_{\text{enc},2})$ and $\langle W_2(\gamma_2)W_2(\gamma_4) \rangle = C_2(t_{\text{enc},1} + t_{\text{enc},2})$. At each of the encounters we take a Poincaré surface of section. The action differences $\Delta\mathcal{S} = \mathcal{S}_{\gamma_2} - \mathcal{S}_{\gamma_1} + \mathcal{S}_{\gamma_3} - \mathcal{S}_{\gamma_4}$ or $\Delta\mathcal{S} = \mathcal{S}_{\gamma_2} - \mathcal{S}_{\gamma_1} + \mathcal{S}_{\gamma_3} - \mathcal{S}_{\gamma_4}$ that appear in the exponents in Eq. (17) are then expressed in terms of the phase space distances s_j and u_j between the two solid trajectories in Fig. 3 along the stable and unstable directions in phase space at each of the encounters, $\Delta\mathcal{S} = s_1 u_1 + s_2 u_2$.^{46,47} The encounter durations $t_{\text{enc},1}$ and $t_{\text{enc},2}$ are expressed in terms of these coordinates as

$$t_{\text{enc},j} = \frac{1}{\lambda} \ln \frac{c^2}{|s_j u_j|}, \quad j = 1, 2. \quad (18)$$

Calculating the trajectory sum as in Refs. 33,38,44,45, we then find

$$\begin{aligned} \langle \Pi^L \Pi^R \rangle_{A1} &= \frac{8\pi^2 N_1 N_2 \tau_D^2}{N^2} \left(\prod_{j=1}^2 \int_0^\infty \frac{d\tau_j}{\tau_D} e^{-\tau_j/\tau_D} \right) \int_{-c}^c ds_1 du_1 ds_2 du_2 \frac{e^{-i(s_1 u_1 + s_2 u_2)/\hbar - (t_{\text{enc},1} + t_{\text{enc},2})/\tau_D}}{(2\pi\hbar)^2 t_{\text{enc},1} t_{\text{enc},2}} \\ &\quad \times C_1 C_2 [(t_{\text{enc},1} + t_{\text{enc},2})(\tau_1 + \tau_2) + \tau_1 \tau_2]. \end{aligned} \quad (19)$$

The factors $t_{\text{enc},1}$ and $t_{\text{enc},2}$ in the denominator in Eq. (19) cancel a spurious contribution from the freedom to take the Poincaré surface of section at an arbitrary point in the encounter region.

We then make the variable change $u_j = c/\sigma_j$, $s_j = cx_j\sigma_j$. In terms of the new variables, one has $t_{\text{enc},j} = \lambda^{-1} \ln(1/|x_j|)$. Performing the integrals over τ_1 , τ_2 , σ_1 , and σ_2 , one then finds

$$\langle \Pi^L \Pi^R \rangle_{A1} = \frac{32N_1 N_2}{N^2} C_1 C_2 \prod_{j=1}^2 \left[r \tau_D \lambda \int_0^1 dx_j x_j^{\frac{1}{\lambda\tau_D}} \cos(rx_j) \right] [2\tau_D(t_{\text{enc},1} + t_{\text{enc},2}) + \tau_D^2], \quad (20)$$

where we abbreviated $r = c^2/\hbar$.

We now turn to compute contributions of type A2. Because the first encounter touches the leads, the encounter duration $t_{\text{enc},1}$ is no longer determined by the phase space coordinates s_1 and u_1 , but becomes an integration variable itself. The integration range for $t_{\text{enc},1}$ is $\lambda^{-1} \ln(c/|u_1|) < t_{\text{enc},1} < \lambda^{-1} \ln(c^2/|u_1 s_1|)$,⁴⁵ so that

$$\begin{aligned} \langle \Pi^L \Pi^R \rangle_{A2} &= \frac{8\pi^2 N_1 N_2 \tau_D^2}{N^2} \left(\prod_{j=1}^2 \int_0^\infty \frac{d\tau_j}{\tau_D} e^{-\tau_j/\tau_D} \right) \int_{-c}^c ds_1 du_1 ds_2 du_2 \int_{\lambda^{-1} \ln c/|u_1|}^{\lambda^{-1} \ln c^2/|s_1 u_1|} \frac{dt_{\text{enc},1}}{\tau_D} \\ &\quad \times \frac{e^{-i(s_1 u_1 + s_2 u_2)/\hbar - (t_{\text{enc},1} + t_{\text{enc},2})/\tau_D}}{(2\pi\hbar)^2 t_{\text{enc},1} t_{\text{enc},2}} C_1 C_2 [(t_{\text{enc},1} + t_{\text{enc},2})(\tau_1 + \tau_2) + \tau_1 \tau_2]. \end{aligned} \quad (21)$$

The second encounter time is still given by Eq. (18) above. As before, we perform the variable change $u_j = c/\sigma_j$, $s_j = cx_j\sigma_j$, $j = 1, 2$. Upon integration over τ_1 , τ_2 , σ_1 , σ_2 , and $t_{\text{enc},1}$ we then find

$$\begin{aligned} \langle \Pi^L \Pi^R \rangle_{A2} &= -\frac{32N_1N_2}{N^2} C_1 C_2 \left[r\tau_D \lambda \int_0^1 dx_2 x_2^{\frac{1}{\lambda\tau_D}} \cos(rx_2) \right] \\ &\times r\tau_D \lambda \int_0^1 dx_1 \cos(rx_1) \left[x_1^{1/\lambda\tau_D} (2\tau_D t_{\text{enc},1} + 2\tau_D t_{\text{enc},2} + 3\tau_D^2) - (2\tau_D t_{\text{enc},2} + 3\tau_D^2) \right]. \end{aligned} \quad (22)$$

Here we reverted to the notation $t_{\text{enc},1} = \lambda^{-1} \ln(1/|x_1|)$ in order to make contact with the result for $\langle \Pi^L \Pi^R \rangle_{A1}$ obtained previously. The second term between the square brackets [...] in the second line of Eq. (22) leads to a rapidly oscillating function of r and will be neglected. Combining the remaining terms with Eq. (20) and taking the limit $\hbar \rightarrow 0$ ($r \rightarrow \infty$) while keeping the ratio τ_E/τ_D fixed, we find

$$\begin{aligned} \langle \Pi^L \Pi^R \rangle_A &= -64 \frac{N_1 N_2}{N^2} C_1 C_2 \tau_D^4 \left[r \lambda \int_0^1 dx x^{1/\lambda\tau_D} \cos(rx) \right]^2 \\ &= -16\pi^2 \frac{N_1 N_2}{N^2} C_1 C_2 \tau_D^2 e^{-2\frac{\tau_E}{\tau_D}}, \end{aligned} \quad (23)$$

where the Ehrenfest time is defined as

$$\tau_E = \frac{1}{\lambda} \ln r = \frac{1}{\lambda} \ln \frac{c^2}{\hbar}. \quad (24)$$

Note that the limit $\hbar \rightarrow 0$ at fixed τ_E/τ_D , taken above, can be realized by narrowing the lead openings such that the dwell time increases. While this procedure may change the trajectories contributing to pumping, their statistical properties should be (almost) unaffected. In particular, the Lyapunov exponent will converge to its value in the closed cavity.

B. contributions of type B

The trajectory configurations of type B provide the dominant contributions to the pumped current at large Ehrenfest times. Each pair (γ_1, γ_2) and (γ_3, γ_4) consists of a ‘short’ trajectory and a ‘long’ trajectory, where the long trajectory differs from the short trajectory by winding once around a periodic orbit, see Fig. 3. (Strictly speaking, one should say that the long trajectory winds one extra time around the periodic orbit, because all trajectories involved will wind multiple times around the periodic orbit if τ_E is much longer than the period τ_p of the periodic orbit.) In the trajectory sum (9), each trajectory can be the short one. Following Ref. 33, we parametrize these configurations by Poincaré surfaces of sections which measure the phase space coordinates (s_1, u_1) and (s_2, u_2) of two short trajectories with respect to the stable and unstable manifolds of the periodic orbit.

It will be useful to define several relevant times. The two short trajectories in the configuration are depicted in Fig. 5. The time for which the short trajectories are correlated with the periodic trajectory (phase space distances smaller than the cutoff c) is denoted $t_{\text{enc},1}$ [for the short trajectory of the pair (γ_1, γ_2)] and $t_{\text{enc},2}$ [for the

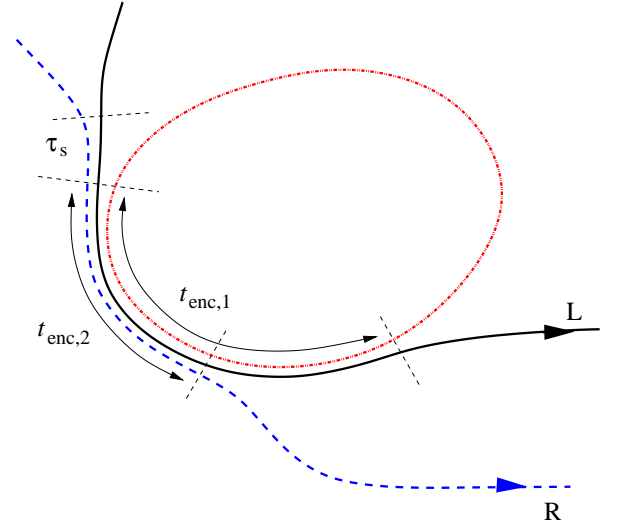


FIG. 5: (Color online) Definitions of the relevant durations for trajectories of type B. The figure shows the short trajectories from each pair, as well as the periodic orbit. The long trajectories from each pair, which are not shown, differ from the short trajectories by one revolution around the periodic orbit. The figure shows the durations $t_{\text{enc},1}$ and $t_{\text{enc},2}$ of the encounters of the short trajectories with the periodic orbit, as well as the time τ_s that the trajectories are correlated before arriving at the periodic orbit. A similar time τ_u measures the time the trajectories are correlated after departure from the periodic orbit. In the example shown in the figure, the trajectories depart at different points, so that $\tau_u = 0$.

short trajectory of the pair (γ_3, γ_4)]. By our construction, the longer trajectory in the pair (not drawn in Fig. 5) will be correlated with the periodic trajectory for a time $t_{\text{enc},j} + \tau_p$, $j = 1, 2$, where τ_p is the period of the periodic orbit. Since the trajectories may leave the neighborhood of the periodic trajectory together, the correla-

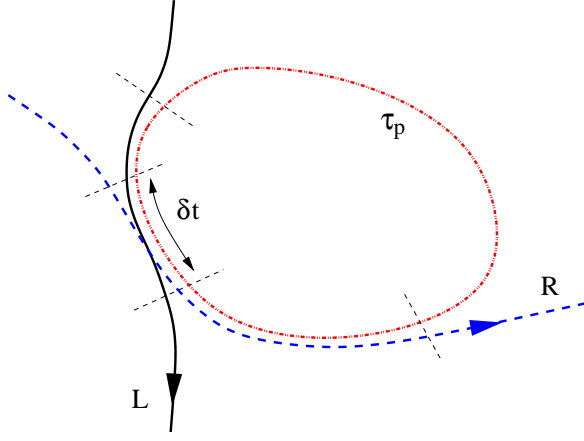


FIG. 6: (Color online) The overlap time is defined as the overlap of the two encounter times $t_{\text{enc},1}$ and $t_{\text{enc},2}$.

tions may extend away from the periodic trajectory. If applicable, we denote the time for which the trajectories are correlated with each other before they arrive to the periodic orbit by τ_s . Similarly, τ_u denotes the eventual correlation time after the trajectories leave the periodic orbit. If $\tau_s \neq 0$, the encounter region extends away from the periodic orbit and may touch the entrance contact. Hence, we distinguish contributions of type B1 and type B2, where type B1 refers to those trajectories for which the encounters fully reside in the quantum dot, and type B2 refers to configurations of trajectories with correlated entry (encounter that touches the entrance lead open-

ing). Since the trajectory pairs (γ_1, γ_2) and (γ_3, γ_4) exit through different contacts, one does not have to consider the possibility that the encounter region touches the exit lead opening. The Poincaré surfaces of section are taken at points where the short trajectories are correlated with the periodic orbit. The distance between the two Poincaré surfaces of section is measured by the travel time t_{12} along the periodic orbit, where we require $|t_{12}| < \tau_p/2$.

Even the shortest trajectory in a pair can wind around the periodic trajectory several times. Thus, it is possible that $t_{\text{enc},j} > \tau_p$. In order to separate out full revolutions, we write

$$t_{\text{enc},j} = n_j \tau_p + \tilde{t}_{\text{enc},j}, \quad (25)$$

where n_j is a non-negative integer and $0 \leq \tilde{t}_{\text{enc},j} < \tau_p$. The use of $\tilde{t}_{\text{enc},j}$ complicates some of the calculations since this time is not a continuous function of the surface of section coordinates. On the other hand, this time appears naturally due to the random Gaussian character of the winding numbers $W_{1,2}$.

Without loss of generality (but with inclusion of a combinatorial factor two), we take γ_1 to be one of the short trajectories. Expanding the product of sines as in Eq. (17), we then see that smallness of the action difference requires γ_3 to be the other short trajectory for the first term in Eq. (17), whereas γ_4 is the other short trajectory in the second term in Eq. (17). In the former case, one has

$$\begin{aligned} \langle W_1(\gamma_1)W_1(\gamma_3) \rangle &= C_1[n_1 n_2 \tau_p + n_1 \tilde{t}_{\text{enc},2} + n_2 \tilde{t}_{\text{enc},1} + \delta\tilde{t} + \tau_s + \tau_u] \\ \langle W_2(\gamma_2)W_2(\gamma_4) \rangle &= C_2[(n_1 + 1)(n_2 + 1)\tau_p + (n_1 + 1)\tilde{t}_{\text{enc},2} + (n_2 + 1)\tilde{t}_{\text{enc},1} + \delta\tilde{t} + \tau_s + \tau_u]. \end{aligned}$$

The time $\delta\tilde{t}$ is the overlap of the ‘remainders’ $\tilde{t}_{\text{enc},1}$ and $\tilde{t}_{\text{enc},2}$, see Fig. 6. In the latter case, one has

$$\begin{aligned} \langle W_1(\gamma_1)W_1(\gamma_3) \rangle &= C_1[n_1(n_2 + 1)\tau_p + n_1 \tilde{t}_{\text{enc},2} + (n_2 + 1)\tilde{t}_{\text{enc},1} + \delta\tilde{t} + \tau_s + \tau_u] \\ \langle W_2(\gamma_2)W_2(\gamma_4) \rangle &= C_2[(n_1 + 1)n_2 \tau_p + (n_1 + 1)\tilde{t}_{\text{enc},2} + n_2 \tilde{t}_{\text{enc},1} + \delta\tilde{t} + \tau_s + \tau_u]. \end{aligned}$$

The resulting contribution of type B1 then reads

$$\begin{aligned} \langle \Pi^L \Pi^R \rangle_{B1} &= 16\pi^2 \frac{N_1 N_2 \tau_D}{N^2} C_1 C_2 \int \frac{d\tau_p}{\tau_D} e^{-\tau_p/\tau_D} \int_{-\tau_p/2}^{\tau_p/2} dt_{12} \int_{-c}^c ds_1 du_1 ds_2 du_2 \frac{e^{i(u_1 s_1 - u_2 s_2)/\hbar - (\tau_s + \tau_u)/\tau_D}}{(2\pi\hbar)^2 t_{\text{enc},1} t_{\text{enc},2}} \\ &\quad \times [\tau_p (\delta\tilde{t} + \tau_s + \tau_u) - \tilde{t}_{\text{enc},1} \tilde{t}_{\text{enc},2}]. \end{aligned} \quad (26)$$

The contributions of type B2 are calculated in a way very similar to the one used for type A2,

$$\begin{aligned} \langle \Pi^L \Pi^R \rangle_{B2} &= 16\pi^2 \frac{N_1 N_2 \tau_D}{N^2} C_1 C_2 \int \frac{d\tau_p}{\tau_D} e^{-\tau_p/\tau_D} \int_{-\tau_p/2}^{\tau_p/2} dt_{12} \int_{-c}^c ds_1 du_1 ds_2 du_2 \frac{e^{i(u_1 s_1 - u_2 s_2)/\hbar - \tau_u/\tau_D}}{(2\pi\hbar)^2 t_{\text{enc},1} t_{\text{enc},2}} \\ &\quad \times \left\{ \left(1 - e^{-\tau_s/\tau_D}\right) [\tau_p (\delta\tilde{t} + \tau_D + \tau_u) - \tilde{t}_{\text{enc},1} \tilde{t}_{\text{enc},2}] - e^{-\frac{\tau_s}{\tau_D}} \tau_p \tau_s \right\}. \end{aligned} \quad (27)$$

Adding both contributions, we then obtain

$$\begin{aligned} \langle \Pi^L \Pi^R \rangle_B &= 16\pi^2 \frac{N_1 N_2 \tau_D}{N^2} C_1 C_2 \int \frac{d\tau_p}{\tau_D} e^{-\frac{\tau_p}{\tau_D}} \int_{-\tau_p/2}^{\tau_p/2} dt_{12} \int_{-c}^c ds_1 du_1 ds_2 du_2 \frac{e^{i(u_1 s_1 - u_2 s_2)/\hbar - \tau_u/\tau_D}}{(2\pi\hbar)^2 t_{\text{enc},1} t_{\text{enc},2}} \\ &\times \left\{ \left(1 - e^{-\tau_s/\tau_D}\right) \tau_p \tau_D + \tau_p (\delta\tilde{t} + \tau_u) - \tilde{t}_{\text{enc},1} \tilde{t}_{\text{enc},2} \right\}. \end{aligned} \quad (28)$$

In App. A it is shown that the contribution from the combination $\tau_p \delta\tilde{t} - \tilde{t}_{\text{enc},1} \tilde{t}_{\text{enc},2}$ between the curly brackets $\{\dots\}$ is of order $C_1 C_2 \tau_D / \lambda$, which can be neglected with respect to $\langle \Pi^L \Pi^R \rangle_A$. The contribution from the term $\tau_p \tau_u$ is a rapidly oscillating function of $r = c^2/\hbar$ and is omitted. The only nonzero contribution arises from the term $\tau_p \tau_D$, which is the only term that is multiplied by both $\exp(-\tau_s/\tau_D)$ and $\exp(-\tau_u/\tau_D)$. This factor $\tau_p \tau_D$ can be taken out of the integral over the phase space variables. The resulting integral was computed in Ref. 33, with the result

$$\begin{aligned} \langle \Pi^L \Pi^R \rangle_B &= -8\pi^2 \frac{N_1 N_2}{N^2} C_1 C_2 \int d\tau_p \tau_p e^{-\tau_p/\tau_D} \\ &\times (1 - e^{-2\tau_E/\tau_D}). \end{aligned} \quad (29)$$

In Eq. (29) we omitted terms proportional to $e^{-\lambda\tau_p}$. Typical periodic trajectories contributing to Eq. (29) have duration $\sim \tau_D$. In the limiting procedure discussed below Eq. (24) these contributions scale as $\exp(-\lambda\tau_D) \rightarrow 0$, justifying this approximation. The integral over the period of the periodic trajectory is easily calculated, resulting in

$$\langle \Pi^L \Pi^R \rangle_B = -8\pi^2 \frac{N_1 N_2}{N^2} C_1 C_2 \tau_D^2 (1 - e^{-2\tau_E/\tau_D}). \quad (30)$$

Combining both contributions together, we find that the total variance of the pumped current is

$$\langle I^2 \rangle = 2 \frac{N_1 N_2}{N^2} \mathcal{A}^2 e^2 \omega^2 C_1 C_2 \tau_D^2 (1 + e^{-2\tau_E/\tau_D}). \quad (31)$$

Equation (31) agrees with random matrix theory in the limit $\tau_E \rightarrow 0$.^{11,23,24} At finite τ_E , the variance of the pumped current is reduced below the random matrix value, but the reduction is not more than a factor two.

When $\tau_E \ll \tau_D$ the pumped current is dominated by trajectories of type A. For $\tau_E \gg \tau_D$ the pumped current is carried by trajectories of type B. Since such trajectory configurations involve a closed loop they are associated with fluctuations of the density of states. Although this scenario is very similar to that of the Ehrenfest-time dependence of the conductance fluctuations, the pumped current has a τ_E -dependent part, whereas the conductance fluctuations in a chaotic quantum dot are fully τ_E independent. The difference occurs, because the mean total duration of the trajectories involved in the internal loop for trajectories of type A is twice the mean duration of the internal loop for trajectories of type B. Conductance fluctuations are insensitive to the loop duration (as

long as the trajectories stay inside the quantum dot), but the pumped current is not.

Equation (31) is valid for systems with and without time reversal symmetry. This is well known in terms of random matrix theory.^{11,23} We have verified this explicitly in the semiclassical approach, see App. B. We also verified that calculation of the current variance using the correlator $\langle (\Pi^L)^2 \rangle$, while technically more involved, gives the same result for the pumped current, as required by unitarity.

IV. NUMERICAL SIMULATION

Despite the remarkable similarity of the semiclassical calculation of the pumped current and the semiclassical calculation of the conductance fluctuations, the former shows a dependence on the Ehrenfest time, whereas the latter does not. In this section we report numerical simulations of the pumped current and compare these with our theoretical predictions.

Because the computational cost of numerical simulation of two-dimensional quantum dots with large Ehrenfest times is prohibitive, Jacquoud, Schomerus, and Beenakker suggested to simulate one dimensional chaotic maps instead.⁴⁸ The phenomenology of chaotic maps is identical to that of chaotic cavities,^{49,50} but the computational cost of simulating a map is significantly lower than that of simulating a cavity. Chaotic maps have been successfully used to study the Ehrenfest time dependence of a range of properties of chaotic quantum dots.^{29,32,48,51,52,53,54,55}

The quantum map propagates a finite state vector of size $M = 1/2\pi\hbar$ in time,

$$\psi(t+1) = \mathcal{F}\psi(t), \quad (32)$$

where \mathcal{F} is the Floquet operator of the map. Assigning two consecutive sets of N_1 and N_2 elements of the vector ψ to contacts, the map can be used to construct a $(N_1 + N_2)$ -dimensional scattering matrix S according to the rule^{48,56}

$$S(\varepsilon) = \mathcal{P} [1 - e^{i\varepsilon} \mathcal{F} \mathcal{Q}]^{-1} e^{i\varepsilon} \mathcal{F} \mathcal{P}^T \quad (33)$$

where \mathcal{P} is a $(N_1 + N_2) \times M$ matrix projecting on the lead sites, $\mathcal{Q} = 1 - \mathcal{P}^T \mathcal{P}$, and ε is the quasi energy.

The map used in our simulations is the 'three-kick quantum rotator',⁵² which is specified by the Floquet operator,

$$\mathcal{F}_{mn} = (XUY^*UYUX)_{mn} \quad (34)$$

where

$$\begin{aligned} Y_{mn} &= \delta_{mn} e^{i(\gamma M/6\pi) \cos(2\pi m/M)}, \\ X_{mn} &= \delta_{mn} e^{-i(M/12\pi)V(2\pi m/M)}, \\ U_{mn} &= M^{-1/2} e^{-i\pi/4} e^{i\pi(m-n)^2/M}. \end{aligned} \quad (35)$$

In this model M is even, but not a multiple of 3. The kick potential is given by

$$V(\theta) = K \cos(\pi q/2) \cos \theta + \frac{1}{2} K \sin(\pi q/2) \sin 2\theta, \quad (36)$$

where q breaks the parity symmetry of the model.⁵⁷ The parameter γ plays the role of a magnetic field resulting in the breaking of time reversal symmetry. This model was used in Refs. 52 and 54 to compute the weak localization correction of the conductance.

There are two parameters in this model: The chaoticity parameter K and the 'magnetic field' γ . We will use K and γ as the time-dependent parameters that drive the quantum pump. Although both K and γ appear in the classical map and thus affect classical trajectories, the variations used in our simulations are sufficiently small that the changes of the classical dynamics can be neglected within the mean dwell time $\tau_D = M/(N_1 + N_2)$.

In the simulations we took equal channel numbers in both contacts, $N_1 = N_2 = N/2$. The semiclassical limit is taken by increasing the dimension $M = 1/2\pi\hbar$ of the system, while keeping the dwell time $\tau_D = M/N$ fixed. This means that N is scaled proportional to M . This way we are certain that there are no variations in the classical dynamics while decreasing \hbar . With these definitions the Ehrenfest time is estimated to be

$$\tau_E \simeq \frac{1}{\lambda} \ln N, \quad (37)$$

plus an N -independent constant. The Lyapunov exponent λ is calculated independently from a simulation of the classical counterpart of the map.

The pumping strength depends on the two parameters C_K and C_γ that describe the rate at which variations of K and γ affect transport. (In the semiclassical theory, these parameters were called C_1 and C_2 .) In order to calculate C_K and C_γ , we first performed separate numerical simulations of the quantities

$$\begin{aligned} y_K &= \sum_{\alpha=1}^{N_1} \sum_{\beta=N_1+1}^N \left| \frac{\partial S_{\alpha\beta}}{\partial K} \right|^2, \\ y_\gamma &= \sum_{\alpha=1}^{N_1} \sum_{\beta=N_1+1}^N \left| \frac{\partial S_{\alpha\beta}}{\partial \gamma} \right|^2, \end{aligned} \quad (38)$$

and compared these to the result of a semiclassical calculation,

$$y_{K,\gamma} = \frac{N_1 N_2}{N} C_{K,\gamma} \tau_D. \quad (39)$$

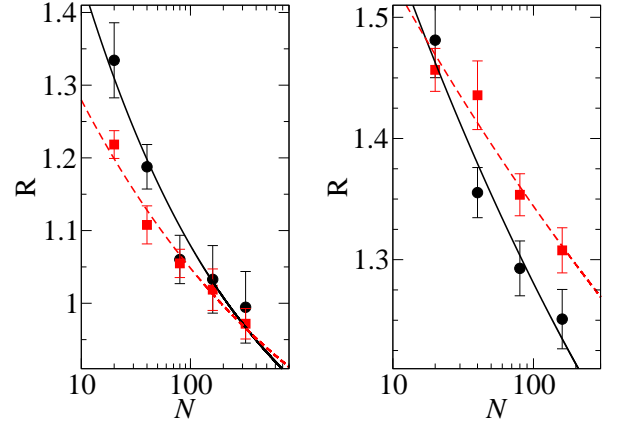


FIG. 7: (Color online) The normalized current variance R , as a function of N . The symbols denote simulation results for the three-kick model with $K = 10$, $q = 0.2$ and $\gamma = 5$ (circles) or $\gamma = 10$ (squares). Results for $\tau_D = 5$ (left panel) and $\tau_D = 10$ (right panel) are shown. The solid and dashed line are fits to theory, as described in text.

We then calculated the kernels Π^L and Π^R numerically, and considered the ratio

$$R = \frac{-N_1 N_2}{8\pi^2} \left\langle \frac{\Pi^L \Pi^R}{y_K y_\gamma} \right\rangle. \quad (40)$$

The prediction of the semiclassical theory is

$$R = 1 + e^{-2\tau_E/\tau_D}. \quad (41)$$

The normalized pumping current variance R is ensemble averaged by variation of the quasi energy ε and lead positions. Since the variation of the lead positions may result in large classical variations, we use the same set of lead positions for different values of M . The factors $\Pi^L \Pi^R$, y_K and y_γ are first averaged over the quasienergy. This average can be done analytically.⁵⁴ Then R is averaged over 2000 different lead positions.

We have checked that when the dwell time is increased the pumping current variance tends to the random matrix limit $R = 2$. (Data not shown. The trend can be seen by comparing the left panel of Fig. 7 [where $\tau_D = 5$] to the right panel [where $\tau_D = 10$].) However, in order to access the regime in which τ_E and τ_D are comparable, we have to take the rather small value of $\tau_D = 5$. In this case, full ergodicity is not achieved during the time τ_D , which results in a deviation from the random matrix limit even for small Ehrenfest times. A similar deviation from random matrix theory was observed in numerical simulations of weak localization and universal conductance fluctuations.^{29,30,31,32,52,53,54}

While the necessity to consider short dwell times prevents a quantitative comparison of simulations and theory, our simulations, which are shown in Fig. 7, show an unambiguous dependence on τ_E . To quantify the dependence we have fitted the simulation results to a function

of the form $R = A + B \exp[-(2/\lambda\tau_D) \ln N]$. The values of the Lyapunov exponent are obtained from a simulation of the classical map⁵² corresponding to (34). We find $\lambda \simeq 1.43$ for $\gamma = 5$ and $\lambda \simeq 2.04$ for $\gamma = 10$. The fit constants are found to be $A \simeq 0.74$ and $B \simeq 1.18$ for $\gamma = 5$ and $\tau_D = 5$; $A \simeq 0.64$ and $B \simeq 1.0$ for $\gamma = 10$ and $\tau_D = 5$; $A \simeq 0.56$ and $B \simeq 1.37$ for $\gamma = 5$ and $\tau_D = 10$; and $A \simeq 0.61$ and $B \simeq 1.15$ for $\gamma = 10$ and $\tau_D = 10$. Deviations from the theoretical values $A = B = 1$ are attributed to the nonuniversal corrections (caused by the small dwell time τ_D). The unknown additive constant in the expression (37) for the Ehrenfest time is absorbed in the parameter B and may cause further deviations from the predicted value $B = 1$.

As mentioned above, the small dwell times used in the simulation cause non-universal and systematic deviations from the theoretical prediction. Increasing the dwell time is numerically expensive. It also strongly suppresses the dependence of R on the number of channels N . With these limitations, we conclude that, while the simulation does not unambiguously confirm the semiclassical theory, it certainly is not inconsistent with it: The data shows a clear dependence on the Ehrenfest time, whereas the nonzero fitted values for A clearly point to a finite value of R in the classical limit $N \rightarrow \infty$.

V. CONCLUSION

In this article we presented a semiclassical theory of the current pumped through a ballistic and chaotic quantum dot with two time-dependent external perturbations. In a quantum pump, the external perturbations couple to the phase of the electronic wavefunction, not to the classical dynamics, so that the pumped current is generated through quantum interference only. Our semiclassical theory identifies the two classes of interfering trajectories that contribute to the root-mean-square current $\text{rms } I = \langle I^2 \rangle^{1/2}$. These are shown in Fig. 3. In each case, the semiclassical contribution for $\langle I^2 \rangle$ originates from two pairs of classical trajectories which meet at small-angle encounters. The interference arises from time-dependent phase differences accumulated between the encounters.

Our semiclassical calculation shows that the action of the external perturbations during the small-angle encounters does not generate a direct current. This follows, *e.g.*, from the final expressions (23) and (29) for the two contributions to the pumped current, which contain the mean times of the interference loops but not the encounter times. Although such a fact appears natural for a quantum interference effect — nontrivial interference can occur only if trajectories are separated in phase space —, within the semiclassical formalism it follows

only after cancellation between contributions of trajectories with and without correlated entry. In this respect, our calculation again emphasizes the necessity to treat trajectory configurations with and without correlated entry on the same footing.^{30,33,45,58}

The main goal of our calculation was to provide a quantitative description of the pumped current if the Ehrenfest time τ_E is comparable to the mean dwell time τ_D in the quantum dot. The Ehrenfest time is the time required for the chaotic classical dynamics to separate two phase space points initially a Fermi wavelength apart to classical distance. As such, τ_E presents a threshold time before which no quantum interference can occur. While we do find that the pumped current is sensitive to the ratio τ_E/τ_D , the pumped current remains nonzero, even in the limit $\tau_E \gg \tau_D$. In the limit $\tau_E \gg \tau_D$, the trajectories that contribute to the pumped current wind many times around a periodic orbit. The escape probability for such a configuration depends on the period of the periodic orbit, not on the total duration of the trajectories involved. This explains why such trajectories continue to exist even if their duration far exceeds the mean dwell time τ_D .

Acknowledgments

We would like to thank Maxim Vavilov for discussions. This work was supported by the NSF under grant no. DMR 0334499 and by the Packard Foundation.

APPENDIX A: REMAINDER TIMES INTEGRATION

In this appendix we show that the integral

$$J = \int d\tau_p e^{-\tau_p/\tau_D} \int_{-\tau_p/2}^{\tau_p/2} dt_{12} \int_{-c}^c ds_1 du_1 ds_2 du_2 \times \frac{e^{i(u_1 s_1 - u_2 s_2)/\hbar - \tau_s/\tau_D}}{\hbar^2 t_{\text{enc},1} t_{\text{enc},2}} [\tau_p \delta \tilde{t} - \tilde{t}_{\text{enc},1} \tilde{t}_{\text{enc},2}], \quad (\text{A1})$$

is of order τ_D/λ . After the replacement of τ_s by τ_u , which is allowed by symmetry, this proves the claim that the terms proportional to $\tau_p \delta \tilde{t} - \tilde{t}_{\text{enc},1} \tilde{t}_{\text{enc},2}$ in the curly brackets $\{\dots\}$ in Eq. (28) does not contribute to the correlator $\langle \Pi^L \Pi^R \rangle$.

First, we point out that the integral over t_{12} vanishes if one omits the factor $\exp[-\tau_s/\tau_D]$ from the expression for J . Hence, we may replace the factor $\exp[-\tau_s/\tau_D]$ in Eq. (A1) by $\exp[-\tau_s/\tau_D] - 1$,

$$J = \int d\tau_p e^{-\tau_p/\tau_D} \int_{-\tau_p/2}^{\tau_p/2} dt_{12} \int_{-c}^c ds_1 du_1 ds_2 du_2 \frac{e^{i(u_1 s_1 - u_2 s_2)/\hbar}}{\hbar^2 t_{\text{enc},1} t_{\text{enc},2}} \left(e^{-\tau_s/\tau_D} - 1 \right) (\tau_p \delta \tilde{t} - \tilde{t}_{\text{enc},1} \tilde{t}_{\text{enc},2}). \quad (\text{A2})$$

The contributions for this integral are from trajectories γ_1 , γ_2 , γ_3 , and γ_4 with correlated arrival at the periodic orbit, since the integrand vanishes if $\tau_s = 0$. On the other hand, the departure from the periodic orbit need not be correlated.

Following Ref. 33 we perform a change of variables using $s_j = c/\sigma_j$, $u_j = cx_j\sigma_j$, $j = 1, 2$, and $t'_{12} = t_{12} - \lambda^{-1} \ln(c/|s_1|) + \lambda^{-1} \ln(c/|s_2|)$. This change of variables amounts to choosing the Poincaré surfaces of section at the point where each trajectory first comes within a phase space distance c from the periodic orbit. The time t'_{12} is the distance between the new Poincaré surfaces of section, measured as the travel time along the periodic orbit. The integrations over σ_j , $j = 1, 2$, can be done, and cancel the factors $t_{\text{enc},j}$ in the denominator. The resulting expression for J is

$$J = 2\lambda^2 r^2 \int d\tau_p e^{-\tau_p/\tau_D} \int_{-\tau_p/2}^{\tau_p/2} dt'_{12} \sum_{\pm} \int_{-1}^1 dx_1 dx_2 \left(e^{-\tau_s/\tau_D} - 1 \right) \cos(rx_1 \mp rx_2) (\tau_p \delta \tilde{t} - \tilde{t}_{\text{enc},1} \tilde{t}_{\text{enc},2}), \quad (\text{A3})$$

where the sum over the signs originates from the possible relative signs between s_1 and s_2 and $r = c^2/\hbar$. We perform another change of variables,³³ defining $u_1 = x_1$, $u_2 = \pm x_2$ and $w = \pm e^{\lambda t'_{12}}$. Both the integration over t'_{12} and the summation over the signs are combined into the integral over w . A straightforward calculation leads to

$$J = 2\lambda r^2 \int d\tau_p e^{-\frac{\tau_p}{\tau_D}} \int \frac{dw}{|w|} \int_{-1}^1 du_1 du_2 \left(e^{-\tau_s/\tau_D} - 1 \right) \times \cos(ru_1 - ru_2) (\tau_p \delta \tilde{t} - \tilde{t}_{\text{enc},1} \tilde{t}_{\text{enc},2}). \quad (\text{A4})$$

In Eq. (A4), the time τ_s depends only on the location where the trajectories in each pair become correlated with the periodic orbit. Following Ref. 33, we set

$$\tau_s = \frac{1}{\lambda} \ln \left[\frac{\max(w, 1/w) - 1}{b - 1} \right], \quad (\text{A5})$$

where b is a numerical constant of order unity. Because of the factor $\exp(-\tau_s/\tau_D) - 1$, only $|w|$ close to unity, corresponding to $\lambda|t'_{12}| \lesssim 1$, contributes to the integral. This implies that the overlap time $\delta \tilde{t}$ can be approximated by

$$\delta \tilde{t} = \min(\tilde{t}_{\text{enc},1}, \tilde{t}_{\text{enc},2}), \quad (\text{A6})$$

where

$$\tilde{t}_{\text{enc},j} = \frac{1}{\lambda} \ln(1/|u_j|) \mod \tau_p. \quad (\text{A7})$$

The terms neglected in this approximation can, at most, lead to corrections of order $1/\lambda\tau_D$.

The integrals over w and u_1, u_2 factorize. Integrating over w gives a factor of order $1/\lambda\tau_D$. The remaining integral over u_1 and u_2 is complicated due to the discontinuity of the encounter times when they reach the period τ_p , see Eq. (A7). We deal with this problem by separating the integral into domains where the integrand is continuous. The integral of the term proportional to $\tilde{t}_{\text{enc},1} \tilde{t}_{\text{enc},2}$ factorizes to a product of two integrals. They

are given by

$$\begin{aligned} J_{1,j} &= r \int_0^1 du_j \cos(ru_j) \tilde{t}_{\text{enc},j} \\ &= \frac{1}{\lambda} \int_0^1 \frac{du_j}{u_j} \sin(ru_j) - \tau_p f(r), \end{aligned} \quad (\text{A8})$$

where

$$f(r) = \sum_{m=0}^{\infty} \sin \left(r e^{-(m+1)\lambda\tau_p} \right). \quad (\text{A9})$$

In the classical limit $r \rightarrow \infty$ and the integral in the first term in Eq. (A8) converges to $\pi/2$. This leads to

$$J_{1,j} = \frac{\pi}{2\lambda} - \tau_p f(r). \quad (\text{A10})$$

For typical periodic orbits $\lambda\tau_p \gg 1$ and thus we expect the second term in (A10) to dominate. Since both r and $e^{\lambda\tau_p}$ are large we expect that the terms in the series $f(r)$ are either rapidly oscillating or small. Averaging over variations of the cut-off r or a local average over λ or τ_p will smear out the oscillating terms. In this case the series converges to some small value. We can conclude that f is at most of order unity, so that $J_{1,j}$ is at most of order τ_p . This suggests that the product $J_{1,1}J_{1,2}$ contributes a term of order τ_p^2 to J . However, we will find that the terms proportional to τ_p^2 cancel and the integral is actually smaller.

It remains to calculate the integral of the term proportional to $\tau_p \delta \tilde{t}$ in Eq. (A4),

$$J_2 = r_1 r_2 \int_0^1 du_1 du_2 \cos(r_1 u_1) \cos(r_2 u_2) \tau_p \delta \tilde{t}. \quad (\text{A11})$$

Again, we separate the integration domain into regions where the integrand is continuous. Rescaling the integration variables as $u_j = y_j e^{-m\lambda\tau_p}$, one finds

$$J_2 = -\frac{r_1 r_2}{\lambda} \sum_{l,m=0}^{\infty} \tau_p e^{-(m+l)\lambda\tau_p} \left\{ \int_{e^{-\lambda\tau_p}}^1 dy_1 \int_{e^{-\lambda\tau_p}}^{y_1} dy_2 \cos(r_1 e^{-m\lambda\tau_p} y_1) \cos(r_2 e^{-l\lambda\tau_p} y_2) \ln y_1 \right. \\ \left. + \int_{e^{-\lambda\tau_p}}^1 dy_1 \int_{y_1}^1 dy_2 \cos(r_1 e^{-m\lambda\tau_p} y_1) \cos(r_2 e^{-l\lambda\tau_p} y_2) \ln y_2 \right\}. \quad (\text{A12})$$

Here we used two a priori different cut-offs r_1 and r_2 for the two integrations, instead of the single cut-off $r = c^2/\hbar$. The use of two different cut-offs is needed to exclude products of oscillating functions of r_1 and r_2 , which would give a non-oscillating contribution to the integral if the same cut-off would have been used. The integral over y_2 in the first term of (A12) can be easily done. Similarly, the integral over y_1 can be done in the second term, with the result

$$J_2 = -\frac{r_1}{\lambda} \sum_{m,l=0}^{\infty} \tau_p e^{-m\lambda\tau_p} \int_{e^{-\lambda\tau_p}}^1 dy \cos(r_1 e^{-m\lambda\tau_p} y) \left[\sin(r_2 e^{-l\lambda\tau_p} y) - \sin(r_2 e^{-(l+1)\lambda\tau_p}) \right] \ln y \\ - \frac{r_2}{\lambda} \sum_{m,l=0}^{\infty} \tau_p e^{-l\lambda\tau_p} \int_{e^{-\lambda\tau_p}}^1 dy \cos(r_2 e^{-l\lambda\tau_p} y) \left[\sin(r_1 e^{-m\lambda\tau_p} y) - \sin(r_1 e^{-(m+1)\lambda\tau_p}) \right] \ln y. \quad (\text{A13})$$

Partial integration results in

$$J_2 = \sum_{l,m=0}^{\infty} \tau_p \int_{e^{-\lambda\tau_p}}^1 \frac{dy}{y} \sin(r_1 e^{-m\lambda\tau_p} y) \sin(r_2 e^{-l\lambda\tau_p} y) + \tau_p^2 f(r_1) f(r_2) - \frac{\pi\tau_p}{2\lambda} [f(r_1) + f(r_2)], \quad (\text{A14})$$

where the function $f(r)$ was defined in Eq. (A9) above.

In order to estimate the series of integrals in Eq. (A14) it is useful to divide the double sum into parts using

$$\sum_{l,m=0}^{\infty} = \sum_{l=m=0}^{\infty} + \sum_{m=0}^{\infty} \sum_{l=m+1}^{\infty} + \sum_{l=0}^{\infty} \sum_{m=l+1}^{\infty},$$

and consider each part separately. The diagonal sum gives

$$\frac{1}{\lambda} \sum_{m=0}^{\infty} \int_{e^{-\lambda\tau_p}}^1 \frac{dy}{y} \sin(r_1 e^{-m\lambda\tau_p} y) \sin(r_2 e^{-m\lambda\tau_p} y) = \frac{1}{\lambda} \int_0^1 \frac{du}{u} \sin(r_1 u) \sin(r_2 u) \\ \rightarrow \frac{1}{2\lambda} \ln \left| \frac{r_1 + r_2}{r_1 - r_2} \right|. \quad (\text{A15})$$

The fact that this integral diverges for $r_1 = r_2$ is an artifact of choosing the same cut-off for both encounters. When the cutoffs differ the resulting expression is finite and of order $1/\lambda$. (Certainly, there are no factors of τ_p .) For the summation with $l > m$ we find

$$\frac{1}{\lambda} \sum_{m=0}^{\infty} \sum_{k=1}^{\infty} \int_{e^{-\lambda\tau_p}}^1 \frac{dy}{y} \sin(r_1 e^{-m\lambda\tau_p} y) \sin(r_2 e^{-(m+k)\lambda\tau_p} y) = \frac{1}{\lambda} \sum_{k=1}^{\infty} \int_0^1 \frac{du}{u} \sin(r_1 u) \sin(r_2 e^{-k\lambda\tau_p} u). \quad (\text{A16})$$

Note that while the argument in the first sine is typically large this may not be the case for the second sine. Let us denote by k_0 the point where the exponential balances r_2 , that is, $r_2 e^{-k_0\lambda\tau_p} = 1$. Typically k_0 is not an integer and $r_2 e^{-[k_0]\lambda\tau_p} \gg 1$ while $r_2 e^{-([k_0]+1)\lambda\tau_p} \ll 1$. For $k < k_0$ both sines are rapidly oscillating and the integral can be approximated by integrating up to infinity. This result in the series

$$\frac{1}{\lambda} \sum_{k=1}^{[k_0]} \int_0^{\infty} \frac{du}{u} \sin(r_1 u) \sin(r_2 e^{-k\lambda\tau_p} u) \simeq \frac{1}{2\lambda} \sum_{k=1}^{[k_0]} \ln \left| \frac{r_1 + r_2 e^{-k\lambda\tau_p}}{r_1 - r_2 e^{-k\lambda\tau_p}} \right| \simeq \frac{1}{\lambda} e^{-\lambda\tau_p}. \quad (\text{A17})$$

For $k > k_0$ we can expand the second sine since its argument is much smaller than unity everywhere in the integration range. As a result one finds

$$\frac{1}{\lambda} \sum_{k=[k_0]+1}^{\infty} r_2 e^{-k\lambda\tau_p} \int_0^1 \sin(r_1 u) du \simeq \frac{1}{\lambda} (1 - \cos r_1) \frac{e^{-([k_0]+1)\lambda\tau_p}}{1 - e^{-\lambda\tau_p}} \quad (\text{A18})$$

This part of the sum is much smaller than the other contributions. The case where $m > l$ is treated in the same

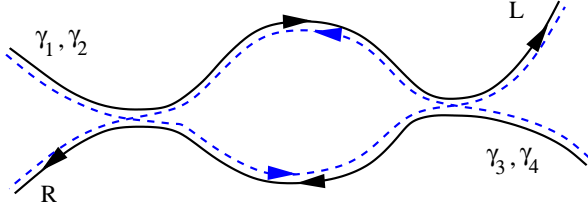


FIG. 8: (Color online) In the presence of time-reversal symmetry one also has to consider interference of time-reversed trajectories. The figure shows the configuration of type A after time-reversal of the trajectories γ_3 and γ_4 .

way. Thus, we can conclude that the series of integrals in Eq. (A14) is of typical size τ_p/λ .

Combining the integrals J_1 and J_2 we find that $J_2 - J_{1,1}J_{1,2}$ is of order τ_p/λ . Since it is in this combination that these integrals enter into the Eq. (A4) for J , we conclude that J is of order τ_D/λ , as advertised.

APPENDIX B: TIME REVERSAL SYMMETRY

The calculation of the pumping current variance performed in Sec. III did not include contributions from trajectory configurations which depend on the presence or absence of time reversal symmetry. Indeed, all stretches of interfering trajectories in Fig. 3 are traversed in the same direction, so that any accumulated phase difference does not depend on an applied magnetic field. For conductance fluctuations, there is an equal contribution to the variance of the conductance in which one pair of trajectories is replaced by the time-reversed trajectories, so that the interfering stretches are traversed in opposite directions, as, *e.g.*, in Fig. 8. (In the language of diagrammatic perturbation theory, such contributions are referred to as ‘Cooperons’.) Such contributions depend

on the presence or absence of time-reversal symmetry and are responsible for the factor-two suppression of $\text{var } G$ upon application of an external magnetic field.^{43,59} For a quantum pump, however, there is no contribution from trajectories that traverse the interference region in opposite directions, so that $\langle I^2 \rangle$ is independent of the presence or absence of time-reversal symmetry. This is well known in terms of random matrix theory.^{11,23} A semiclassical derivation of this fact is given below.

The contribution of type A to the correlator $\langle \Pi^L \Pi^R \rangle$ is shown in Fig. 8, but with the trajectories γ_3 and γ_4 replaced by their time-reversed. The main difference between this configuration of trajectories and configurations which do not depend on time reversal symmetry is that the trajectories in the central loop propagate in opposite directions. We’ll now show that the contribution of such a configuration of classical trajectories to $\langle \Pi^L \Pi^R \rangle$ is zero, even in the absence of an applied magnetic field.

We first consider the contribution of the type “A1”, in which both encounter regions fully reside inside the quantum dot. For this contribution, the reversal of the direction of two of the trajectories has no effect, and one finds that this contribution is given by Eq. (20) of Sec. III. For the configuration depicted in Fig. 8 both encounters can touch the leads, resulting in three additional contributions to $\langle \Pi^L \Pi^R \rangle$. Each of the configurations in which only one encounter touches the lead openings has a contribution given by Eq. (22) of Sec. III (up to the interchange $t_{\text{enc},1} \leftrightarrow t_{\text{enc},2}$ in one of these). The last contribution, from trajectory configurations in which both encounters touch the leads, was not considered in Sec. III. In such a configuration, γ_1 and γ_2 enter through the right contact and γ_3 and γ_4 to enter through the left contact. The calculation of this contribution is similar to that of the contribution “A2” in Sec. III, but with integrations over two encounter times instead of only one. Labeling this configuration “A4”, we find

$$\begin{aligned} \langle \Pi^L \Pi^R \rangle_{A4} = & \frac{32N_1N_2\tau_D^3}{N^2} C_1 C_2 r^2 \lambda^2 \int_0^1 dx_1 dx_2 \cos(rx_1) \cos(rx_2) \\ & \times \left\{ 5\tau_D \left(1 - x_1^{1/\lambda\tau_D} \right) \left(1 - x_1^{1/\lambda\tau_D} \right) - 2t_{\text{enc},2} x_2^{1/\lambda\tau_D} \left(1 - x_1^{1/\lambda\tau_D} \right) - 2t_{\text{enc},1} x_1^{1/\lambda\tau_D} \left(1 - x_2^{1/\lambda\tau_D} \right) \right\}, \end{aligned} \quad (\text{B1})$$

where $t_{\text{enc},j} = (1/\lambda) \ln(1/x_j)$, $j = 1, 2$. Combining all contributions we then find that the additional contribution to the correlator $\langle \Pi^L \Pi^R \rangle$ in the presence of time-reversal symmetry is

$$\langle \Pi^L \Pi^R \rangle_A^{\text{TRS}} = \frac{32N_1N_2\tau_D^4}{N^2} C_1 C_2 r^2 \lambda^2 \int_0^1 dx_1 dx_2 \cos(rx_1) \cos(rx_2) \left(2x_1^{1/\lambda\tau_D} + 2x_2^{1/\lambda\tau_D} - 5 \right). \quad (\text{B2})$$

Upon integration over x_1 and x_2 , all three terms between brackets yield fast oscillating functions of $r = c^2/\hbar$, which are neglected in the classical limit. The calculation of

contributions of type B proceeds along in exactly the same way. We have verified that the resulting contribution can also be neglected.

- ¹ H. Pothier, P. Lafarge, C. Urbina, D. Esteve, and M. H. Devoret, *Europhysics Letters* **17**, 249 (1992).
- ² J. M. Martinis, M. Nahum, and H. D. Jensen, *Phys. Rev. Lett.* **72**, 904 (1994).
- ³ J. E. Avron, A. Elgart, G. M. Graf, and L. Sadun, *Phys. Rev. Lett.* **87**, 236601 (2001).
- ⁴ M. Switkes, C. M. Marcus, K. Campman, and A. C. Gosard, *Science* **238**, 1907 (1999).
- ⁵ D. J. Thouless, *Phys. Rev. B* **27**, 6083 (1983).
- ⁶ V. I. Fal'ko and D. E. Khmelnitskii, *Zh. Eksp. Teor. Fiz.* **95**, 328 (1989) [*Sov. Phys. JETP* **68**, 184 (1989)].
- ⁷ A. A. Bykov, G. M. Gusev, Z. D. Kvon, D. I. Lubyshev, and V. P. Migal, *Pis'ma Zh. Eksp. Teor. Fiz.* **49**, 13 (1989) [*JETP Lett.* **49**, 13 (1989)].
- ⁸ Q. Niu, *Phys. Rev. Lett.* **64**, 1812 (1990).
- ⁹ B. Spivak, F. Zhou, and M. T. Beal Monod, *Phys. Rev. B* **51**, 13226 (1995).
- ¹⁰ J. Ebbecke, N. E. Fletcher, T. J. B. M. Janssen, F. J. Ahlers, M. Pepper, H. E. Beere, and D. A. Ritchie, *Appl. Phys. Lett.* **84**, 4319 (2004).
- ¹¹ P. W. Brouwer, *Phys. Rev. B* **58**, 10135 (1998).
- ¹² B. L. Altshuler and L. I. Glazman, *Science* **283**, 1864 (1999).
- ¹³ F. Zhou, B. Spivak, and B. L. Altshuler, *Phys. Rev. Lett.* **82**, 608 (1999).
- ¹⁴ P. W. Brouwer, *Phys. Rev. B* **63**, 121303 (2001).
- ¹⁵ L. DiCarlo, C. M. Marcus, and J. S. Harris Jr, *Phys. Rev. Lett.* **91**, 246804 (2003).
- ¹⁶ J. N. H. J. Cremers and P. W. Brouwer, *Phys. Rev. B* **64**, 115333 (2002).
- ¹⁷ M. Moskalets and M. Büttiker, *Phys. Rev. B* **64**, 20130 (2001).
- ¹⁸ I. L. Aleiner and A. I. Larkin, *Phys. Rev. B* **54**, 14423 (1996).
- ¹⁹ I. L. Aleiner and A. I. Larkin, *Phys. Rev. E* **55**, R1243 (1997).
- ²⁰ G. M. Zaslavsky, *Phys. Rep.* **80**, 157 (1981).
- ²¹ A. I. Larkin and Y. N. Ovchinnikov, *Zh. Eksp. Teor. Fiz.* **55**, 2262 (1968) [*Sov. Phys. JETP* **28**, 1200 (1969)].
- ²² M. Martinez-Mares, C. H. Lewenkopf, and E. R. Mucciolo, *Phys. Rev. B* **69**, 085301 (2004).
- ²³ T. A. Shutenko, I. L. Aleiner, and B. L. Altshuler, *Phys. Rev. B* **61**, 10366 (2000).
- ²⁴ M. G. Vavilov, V. Ambegaokar, and I. L. Aleiner, *Phys. Rev. B* **63**, 195313 (2001).
- ²⁵ M. L. Polianski, M. G. Vavilov, and P. W. Brouwer, *Phys. Rev. B* **65**, 245314 (2002).
- ²⁶ M. L. Polianski and P. W. Brouwer, *J. Phys. A* **36**, 3215 (2003).
- ²⁷ M. G. Vavilov, L. DiCarlo, and C. M. Marcus, *Phys. Rev. B* **71**, 241309 (pages 4) (2005).
- ²⁸ I. Adagideli, *Phys. Rev. B* **68**, 233308 (2003).
- ²⁹ S. Rahav and P. W. Brouwer, *Phys. Rev. Lett.* **95**, 056806 (2005).
- ³⁰ P. Jacquod and R. S. Whitney, *Phys. Rev. B* **73**, 195115 (2006).
- ³¹ J. Tworzydło, A. Tajic, and C. W. J. Beenakker, *Phys. Rev. B* **69**, 165318 (2004).
- ³² P. Jacquod and E. V. Sukhorukov, *Phys. Rev. Lett.* **92**, 116801 (2004).
- ³³ P. W. Brouwer and S. Rahav, *Phys. Rev. B* **74**, 075322 (2006).
- ³⁴ C. Tian and A. I. Larkin, *Phys. Rev. B* **70**, 035305 (2004).
- ³⁵ P. W. Brouwer, S. Rahav, and C. Tian, *nlin.CD/0607025*.
- ³⁶ M. V. Berry, *Proc. R. Soc. London A* **400**, 229 (1985).
- ³⁷ K. Richter and M. Sieber, *Phys. Rev. Lett.* **89**, 206801 (2002).
- ³⁸ S. Heusler, S. Müller, P. Braun, and F. Haake, *Phys. Rev. Lett.* **96**, 066804 (2006).
- ³⁹ R. A. Jalabert, H. U. Baranger, and A. D. Stone, *Phys. Rev. Lett.* **65**, 2442 (1990).
- ⁴⁰ H. U. Baranger, R. A. Jalabert, and A. D. Stone, *Phys. Rev. Lett.* **70**, 3876 (1993).
- ⁴¹ H. U. Baranger, R. A. Jalabert, and A. D. Stone, *Chaos* **3**, 665 (1993).
- ⁴² M. V. Berry and M. Robnik, *J. Phys. A: Math. Gen.* **19**, 649 (1986).
- ⁴³ A. D. Stone, in *Mesoscopic Quantum Physics*, edited by E. Akkermans, G. Montambaux, J.-L. Pichard, and J. Zinn-Justin (North-Holland, 1995).
- ⁴⁴ P. Braun, S. Heusler, S. Müller, and F. Haake, *cond-mat/051192*.
- ⁴⁵ P. W. Brouwer and S. Rahav, *Phys. Rev. B* **74**, 085313 (2006).
- ⁴⁶ D. Spehner, *J. Phys. A* **36**, 7269 (2003).
- ⁴⁷ M. Turek and K. Richter, *J. Phys. A* **36**, L455 (2003).
- ⁴⁸ P. Jacquod, H. Schomerus, and C. W. J. Beenakker, *Phys. Rev. Lett.* **90**, 207004 (2003).
- ⁴⁹ S. Fishman, D. R. Grempel, and R. E. Prange, *Phys. Rev. Lett.* **49**, 509 (1982).
- ⁵⁰ F. M. Izrailev, *Phys. Rep.* **196**, 299 (1990).
- ⁵¹ J. Tworzydło, A. Tajic, H. Schomerus, and C. W. J. Beenakker, *Phys. Rev. B* **68**, 115313 (2003).
- ⁵² J. Tworzydło, A. Tajic, and C. W. J. Beenakker, *Phys. Rev. B* **70**, 205324 (2004).
- ⁵³ J. Tworzydło, A. Tajic, H. Schomerus, P. W. Brouwer, and C. W. J. Beenakker, *Phys. Rev. Lett.* **93**, 186806 (2004).
- ⁵⁴ S. Rahav and P. W. Brouwer, *Phys. Rev. B* **73**, 035324 (2006).
- ⁵⁵ H. Schomerus and P. Jacquod, *J. Phys. A* **38**, 10663 (2005).
- ⁵⁶ Y. V. Fyodorov and H.-J. Sommers, *JETP Lett.* **72**, 422 (2000).
- ⁵⁷ R. Blümel and U. Smilansky, *Phys. Rev. Lett.* **69**, 217 (1992).
- ⁵⁸ R. S. Whitney and P. Jacquod, *Phys. Rev. Lett.* **96**, 206804 (2006).
- ⁵⁹ B. L. Altshuler and B. D. Simons, in *Mesoscopic Quantum Physics*, edited by E. Akkermans, G. Montambaux, J.-L. Pichard, and J. Zinn-Justin (North-Holland, 1995).